Provided for non-commercial research and education use.
Not for reproduction, distribution or commercial use.

This article appeared in a journal published by Elsevier. The attached copy is furnished to the author for internal non-commercial research and education use, including for instruction at the authors institution and sharing with colleagues.

Other uses, including reproduction and distribution, or selling or licensing copies, or posting to personal, institutional or third party websites are prohibited.

In most cases authors are permitted to post their version of the article (e.g. in Word or Tex form) to their personal website or institutional repository. Authors requiring further information regarding Elsevier's archiving and manuscript policies are encouraged to visit:

http://www.elsevier.com/copyright

Author's personal copy

European Polymer Journal 46 (2010) 2275–2281

Contents lists available at ScienceDirect

European Polymer Journal

journal homepage: www.elsevier.com/locate/europolj

SANS from Pluronic P85 in d-water

Boualem Hammouda

National Institute of Standards and Technology, Center for Neutron Research, 100 Bureau Drive, Gaithersburg, MD 20899, USA

ARTICLE INFO

Article history:
Received 3 August 2010
Received in revised form 29 September 2010
Accepted 5 October 2010
Available online 27 October 2010

Keywords:
Pluronics
Phase transitions
Small-angle neutron scattering
SANS
Polymeric micelles

ABSTRACT

Small-angle neutron scattering (SANS) has been used to investigate Pluronic P85 ($EO_{26}PO_{40}EO_{26}$) copolymer in deuterated water. A range of P85 fractions were measured for a wide sample temperature window. A rich phase behavior is reported. Unimers were observed below the critical micelle formation condition. At fixed P85 fraction, a number of micellar phases were observed upon increasing temperature; first spherical micelles, then cylindrical micelles, then lamellar micelles. At the highest temperature, a demixed lamellae phase was observed. Analysis of the SANS data consisted in fits to an empirical Guinier–Porod model that was appropriate for data fitting in the various phases at low P85 fractions. When the P85 fraction increased, an inter-particle structure factor was included to analyze SANS data from concentrated spherical micelles. At high P85 fractions, paracrystalline structures were observed as evidenced by an enhanced inter-particle interaction peak. A phase diagram for P85/d-water was obtained showing the various phases. Focusing on the spherical micelles phase for one sample composition, a core-shell model was used to fit SANS data and obtain sizes and scattering length densities. Using material balance equations, information such as the aggregation number (i.e., number of Pluronic macromolecules per micelle) and the number of hydration water molecules in the shell region are determined.

Published by Elsevier Ltd.

1. Introduction

Pluronics are triblock copolymers containing poly(propylene oxide) and poly(ethylene oxide) blocks. PEO is the simplest water-soluble polymer; the chemical structure of its monomer $–CH_2CH_2O–$ gives the just-right balance between hydrophobic and hydrophilic interactions to make it soluble in water at ambient temperature. Its neighbor in the homologous series PPO dissolves at low temperatures, but does not dissolve at ambient temperature. This amphiphilic character of Pluronics leads to micelle formation.

Pluronics have been the subject of much research owing to their interesting behavior as unimers (dissolved copolymers) at low temperatures and as micelles at ambient and higher temperatures. Pluronics are used in the pharmaceutical industry in such processes as emulsification, solubilization and dispersion and as agents for thickening, coating and wetting functions. Their biocompatibility makes them appealing additives in drug delivery formulations. The phase behavior of one Pluronic is of interest here.

2. Pluronic samples and measurement method

A Pluronic triblock copolymer corresponding to $EO_{26}PO_{40}EO_{26}$ and referred to as P85 has been obtained from BASF and used with no further treatment. Its molecular weight is around 4600 g/mol as reported by the supplier. P85 samples corresponding to a number of weight fractions were dissolved in deuterated water (d-water) and measured by small-angle neutron scattering (SANS) at various sample temperatures.

SANS measurements were taken on the NG3 instrument at the National Institute of Standards and Technology, Center for Neutron Research (NCNR). Three instrument configurations using 6 Å neutron wavelength were measured in each case; these correspond to low-*Q*, intermediate-*Q*

E-mail address: hammouda@nist.gov

0014-3057/$ - see front matter Published by Elsevier Ltd.
doi:10.1016/j.eurpolymj.2010.10.012

Author's personal copy

and high-Q yielding a scattering variable range between $0.004\ Å^{-1} < Q < 0.4\ Å^{-1}$. Standard data acquisition and reduction procedures were followed in order to obtain corrected and radially averaged SANS macroscopic scattering cross sections.

The P85 weight fractions that were measured went from very dilute (0.2%, 0.5%, 0.7%) to dilute and intermediate (1%, 1.8%, 2%, 3 %, 4%, 5%, 6%) to concentrated fractions (12%, 26%, 47%). These are weight fractions (g/g). SANS data were taken for a wide temperature range (7–98 °C).

The SANS intensity is seen to increase with increasing temperature but the shape of the form factor changes from unimers (at low temperatures) to spherical micelles, then to cylindrical micelles and finally to lamellar micelles upon heating. This is a rich phase behavior accompanied by structural transitions which are deduced based on standard clues from the SANS spectra.

The unimers phase has a characteristic scattering that decays at $1/Q^m$ with m between 1.5 and 1.7 depending on P85 fraction and temperature in the intermediate-Q Porod region; this behavior represents fully swollen polymer chains with slight stiffness. Above the critical micelle temperature (CMT), spherical micelles form. These are characterized by an almost flat signal in the low-Q region and a decrease as $1/Q^4$ in the (intermediate-Q) Porod region. Upon further temperature increase, the low-Q signal increases to yield a $1/Q$ low-Q Porod behavior and a $1/Q^4$ intermediate-Q Porod behavior characteristic of cylindrical micelles that are very long (note the low-Q Guinier region is not observed in the measured window) but have finite radius. At even higher sample temperatures, the SANS data trend changes again to show the lamellar micelles phase. The low-Q Porod behavior changes to $1/Q^2$ which is characteristic of scattering from lamellae. At the highest temperatures, a demixed lamellae phase forms as evidenced by the appearance of an inter-lamellar Bragg peak that represents the inter-lamellar thickness. This new phase is not referred to as a "vesicles" phase since there is no evidence that the formed structures are spherical. Measurements made from sampled bottom and top parts of the sample showed that this demixed lamellae phase does not correspond to complete polymer demixing. It corresponds to demixed lamellae isolating pockets of solvent.

The 0.5% P85/d-water sample shows transitions from the unimers phase at 11 and 21 °C to the spherical micelles phase for temperatures between 40 and 59 °C, then to the cylindrical micelles phase for temperatures between 68 and 78 °C, then to the lamellar micelles phase for 87 °C, and finally to the demixed lamellae phase at 98 °C as shown in Fig. 1. Note that the reported temperatures are the actual (measured) sample temperatures and that the boiling temperature for d-water is around 101 °C.

A simple qualitative data analysis approach which consists in plotting the SANS intensity at low-Q with increasing temperature is used to map out the phase transitions trend in Fig. 2. The low Q value of $0.02\ Å^{-1}$ is used in order to avoid the clustering signal observed at low temperatures completely.

3. The unimers phase

The low P85 weight fractions and low temperatures allow the investigation of the unimers phase. Fig. 3 shows SANS data for 11 °C for a number of low P85 fractions below the critical micelle formation condition. The intermediate-Q signal is characteristic of P85/d-water solvation (hydration) interactions. The low-Q signal shows some clustering. The high-Q incoherent background increases because of the increased amount of hydrogen in the sample due to the increased P85 fraction. Note that there is

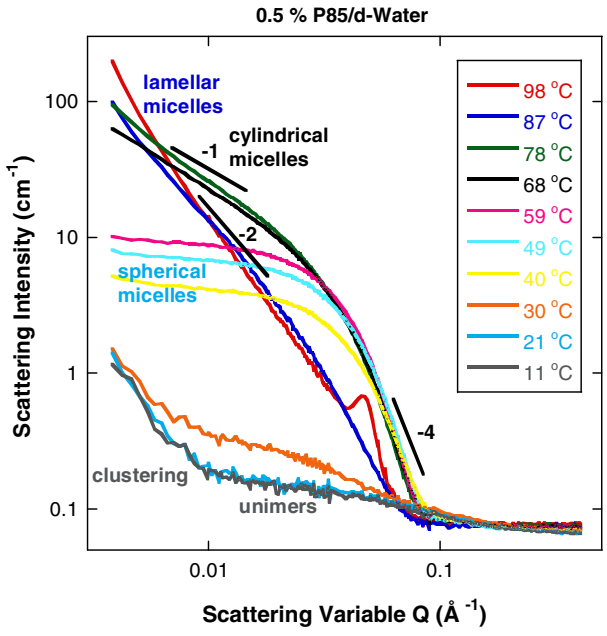

Fig. 1. Reduced SANS data from 0.5% P85 Pluronic in d-water for temperatures between 11 and 98 °C. The Porod slopes have been included (−4 at intermediate-Q and either −1 for cylindrical micelles or −2 for lamellar micelles at low-Q).

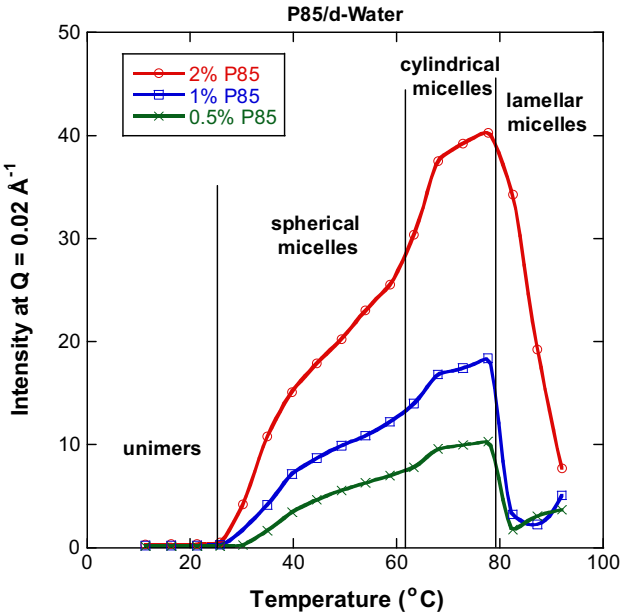

Fig. 2. Variation of a low-Q SANS intensity (taken at $Q = 0.02\ Å^{-1}$) with increasing temperature for the three low weight fraction P85 samples in d-water.

Author's personal copy

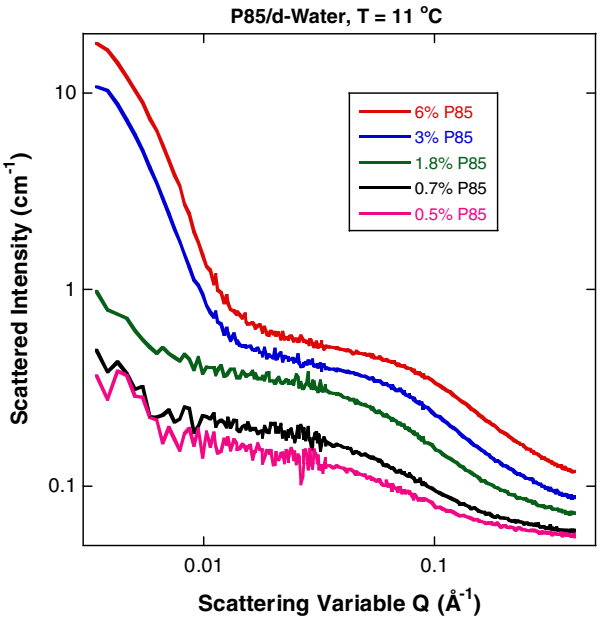

Fig. 3. SANS data from P85/d-water in the unimers phase (low P85 fractions and low temperature of 11 °C).

not enough neutron contrast between the PEO and PPO blocks in the P85 copolymer so that the SANS data in the unimers phase does not contain a correlation hole peak.

4. Micelle formation

When the P85 fraction is above a critical micelle concentration (CMC) and the sample temperature is above a critical micelle temperature (CMT), micelles form. This is characterized by a jump in the SANS intensity as shown in Fig. 2. Since the transitions are not well defined in Fig. 2, another method using an empirical Guinier–Porod model is used to analyze the scattering data.

The empirical Guinier–Porod model uses the following functional forms [1]:

$$I(Q) = \frac{G}{Q^s}\exp\left[\frac{-Q^2R_g^2}{3-s}\right] \text{ for } Q \leqslant Q_1$$
$$I(Q) = \frac{D}{Q^m} \text{ for } Q \geqslant Q_1. \quad (1)$$

R_g is the radius of gyration. This is based on the generalized Guinier law that applies to globular as well as elongated objects such as cylinders or lamellae [2]. For spheres $s = 0$, for cylinders $s = 1$ and for lamellae $s = 2$.

Applying the continuity constraint of the Guinier and Porod functions and their derivatives yields the following relations for the transition point Q_1:

$$Q_1 = \frac{1}{R_g}\sqrt{\frac{(m-s)(3-s)}{2}}$$
$$D = G\exp\left[\frac{-Q_1^2R_g^2}{3-s}\right]Q_1^{(m-s)}. \quad (2)$$

Using this model, nonlinear least-squares fits to the SANS data were performed to obtain the fitting parameters (G, R_g, s, and m) in each case.

Fig. 4 shows the SANS data and fits to the Guinier–Porod model for 0.5% P85/d-water at 11 °C (unimers), 49 °C (spherical micelles), 68 °C (cylindrical micelles) and 87 °C (lamellar micelles). The high-Q incoherent background was not included in the fits. Note that the unimers phase consists of semiflexible polymers as evidenced by Porod exponents between 1.5 and 1.7. These are not Gaussian coils.

Using these results, variation of the low-Q Guinier intensity (first term in Eq. (1)) is plotted for $Q = 0.004$ Å^{-1} in Fig. 5 for the dilute P85 fractions. This method shows clearer transition regions between the unimers phase and the various micellar phases (spherical, cylindrical and lamellar).

The Guinier–Porod model yields a radius of gyration R_g which is related to the size of the scattering objects. The spherical micelles have a radius $R = R_g\sqrt{5/3}$. The cylindrical micelles have a cross sectional radius $R = R_g\sqrt{2}$, their length is outside of the measurement window (longer than 1500 Å). The thickness of the lamellar micelles is given by $T = R_g\sqrt{12}$. Their lateral extent is also outside of the measurement window.

Another way to separate out the various phases is by plotting the variation of the radius of gyration with temperature. This is a good monitor of structural phase transitions. A generic half-size is defined as $(S/2) = R_g\sqrt{(5-s)/(3-s)}$. For spheres, $s = 0$, and $S/2$ is the sphere radius $(S/2) = R = R_g\sqrt{5/3}$. For cylinders, $s = 1$, and $S/2$ is the cross sectional radius $(S/2) = R = R_g\sqrt{2}$. For lamellae, $s = 2$ and $S/2$ is half the cross sectional thickness $(S/2) = (T/2) = R_g\sqrt{12}/2 = R_g\sqrt{3}$ so that $T = R_g\sqrt{12}$. The radius of gyration R_g and the generic half-size $(S/2)$ are plotted in Fig. 6 for the 0.5% P85/d-water at various temperatures.

Note that the observed phase transitions are reversible in temperature. The same phases are obtained upon

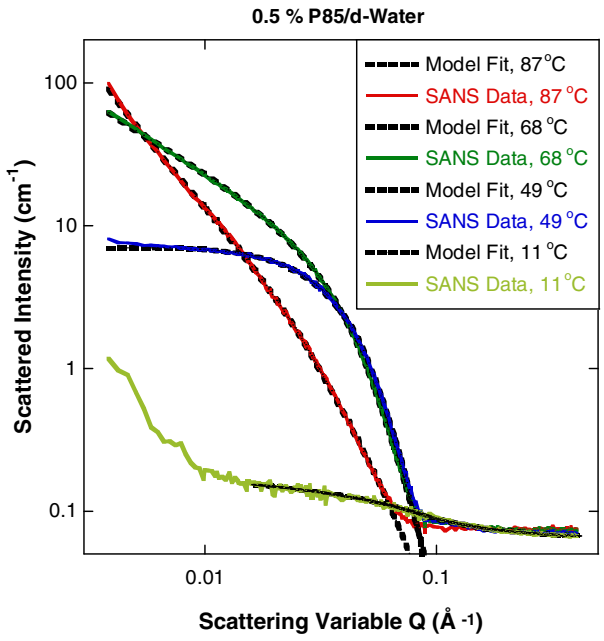

Fig. 4. SANS data and fits to the Guinier–Porod model for 0.5% P85/d-water. The fitting region was chosen to stop just before the flat incoherent background starts. The low-Q clustering region was excluded from the fit for 11 °C.

Author's personal copy

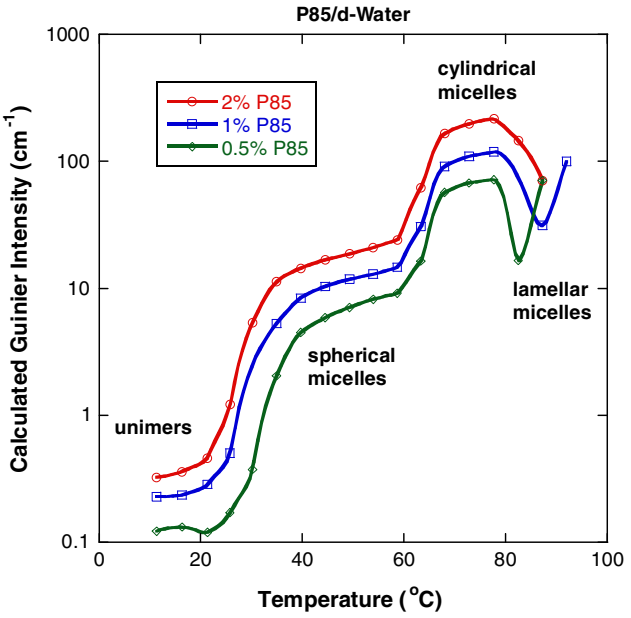

Fig. 5. Variation of the Guinier intensity (at $Q = 0.004$ Å^{-1}) with sample temperature for three dilute P85 fractions.

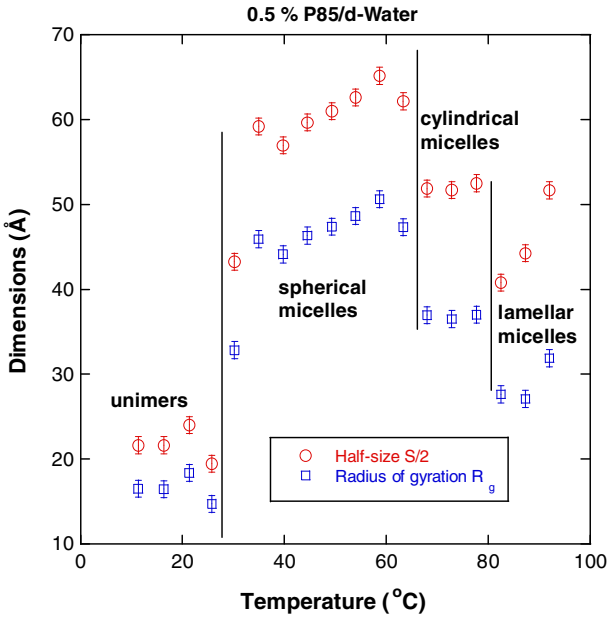

Fig. 6. Variation of the radius of gyration and generic half-size delimiting the various phases. The statistical error bars correspond to one standard deviation.

heating or upon cooling provided that enough sample equilibration time is allowed. Data analysis has so far concentrated on understanding the unimers phase and the various micellar phases in the dilute region. As the P85 fraction is increased, an inter-particle interaction peak develops in the SANS data and another method is needed for data analysis.

5. Higher P85 fractions

Inter-particle interaction peaks are hard to model. For spherical micelles, the Percus–Yevick closure of the Ornstein–Zernike equation offers a compact analytical form for the structure factor. This approximate model is used to generalize the Guinier–Porod model for higher concentrations in the spherical micelles phase region. The scattering cross section is given by [5]:

$$\frac{d\Sigma(Q)}{d\Omega} = \Delta\rho^2 \phi V_P P(Q) S_I(Q). \quad (3)$$

Here $\Delta\rho^2$ is the contrast factor, ϕ is the volume fraction, V_P is the micelle volume, $P(Q)$ is the form factor and $S_I(Q)$ is the structure factor. Note that Eq. (1) with $s = 0$ (for spheres) corresponds to $G = \Delta\rho^2\phi\ V_P P(Q)$ when $S_I(Q) = 1$ (i.e., in the dilute limit).

Fig. 7 shows SANS data and model fit for 6% P85/d-water.

Fig. 8 summarizes the SANS data characterizing the unimers phase with the intermediate-Q solvation feature and the low-Q clustering feature. The solvation signal is due to solvent–polymer interactions whereby d-water molecules hydrate the polymer chains. Spherical micelles start forming at 21 °C and are well-formed by 26 °C. Note that the clustering feature disappears as soon as the spherical micelles form. Clustering and micelle formation vary in opposite trends. The clustering feature is the signature of a large network of P85 chains physically linked through hydrophobic interactions.

Fig. 9 shows SANS data from a concentrated sample (26% P85/d-water). The familiar phases can be observed. At 11 °C, the spherical micelles start forming. At 49 °C, the spherical micelles are well-formed and are packed into a "paracrystalline" structure. This is evidenced by the high inter-particle interaction peak height. A phenomenological Hansen–Verlet criterion [3] states that a paracrystalline structure forms when the height of the first peak in the structure factor exceeds a ceiling value (between 2 and 3). This is in comparison to the formation of crystalline

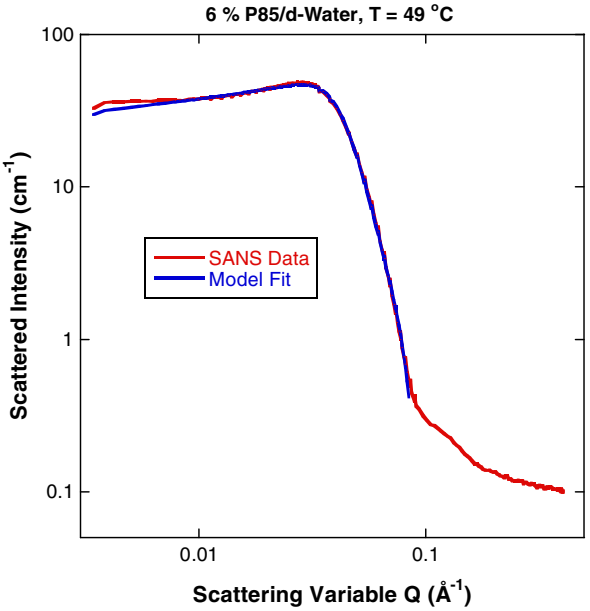

Fig. 7. Model fit and SANS data for 6% P85/d-water at 49 °C (spherical micelles). The empirical Guinier–Porod model was used for the form factor and the Percus–Yevick model was used for the structure factor.

Author's personal copy

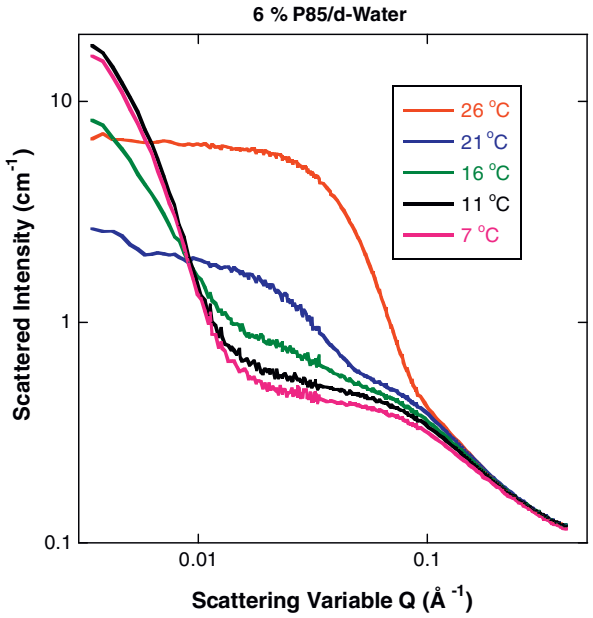

Fig. 8. SANS data from 6% P85/d-water.

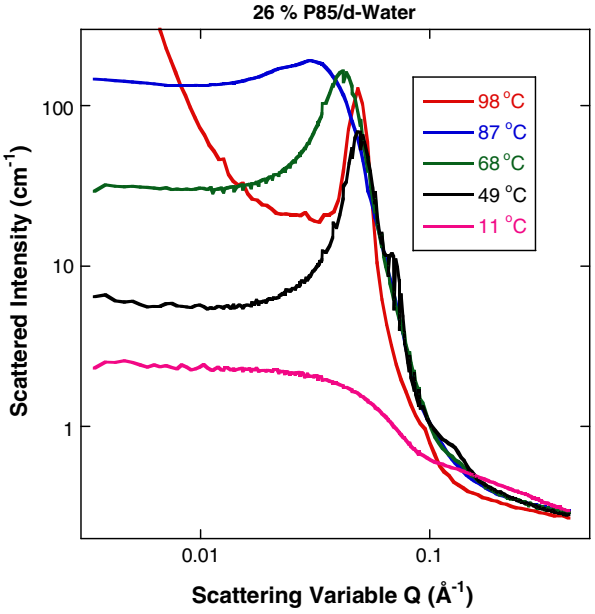

Fig. 9. SANS data from 26% P85/d-water. The observed "oscillations" are due to a lag in temperature equilibration. By the time, the low-Q SANS data were measured, the sample temperature had changed slightly. The intermediate-Q data samples both temperature histories. The demixed lamellae phase forms even at low P85 fractions.

structures from amorphous ones. At 68 °C, a concentrated cylindrical micelles phase is formed. At 87 °C, a lamellar micelles phase is formed. The peak position moves to lower Q due to the increasing inter-micellar size. As temperature is increased, PPO then PEO become more hydrophobic and exclude more water thereby increasing inter-micellar size. At 97 °C, so much water is excluded that a demixed lamellae phase is formed whereby lamellae form partitions between water regions. The micellar phases are driven by the copolymer nature of P85 (hydrophobic PPO and hydrophilic PEO) while the demixed lamellae phase is reached when PEO itself becomes hydrophobic (phase separates) at high temperature. This occurs when PEO hydration (solvation) breaks down due to the breaking of hydrogen bonds.

The various pieces are coming together in order to produce a phase diagram.

6. Branch of the P85/d-water phase diagram

Based on the various intensity jump clues and on the data fitting parameters (the radius of gyration and the Porod exponent), a phase diagram is obtained for P85/d-water. The various phases are well defined. The 47% P85 fraction sample was not included since it is dominated by paracrystalline structures that are impossible to fit using our data analysis approach. Moreover, both PEO and PPO crystallize at high weight fractions. The phase diagram produced in Fig. 10 stops well below the P85 fraction where crystallization occurs.

The qualitative features of this phase diagram agree with a previously published version by Mortensen [4]. Note that the phase boundaries between the various micellar phases are characterized by gentler slopes in the present phase diagram and the demixed lamellae phase was not reported in the previous phase diagram.

7. Core-shell spherical micelles

The spherical micelles phase region is singled out for further in-depth analysis for the 10% P85/d-water sample at various temperatures (from 21 to 59 °C). A spherical core-shell model is used to describe the spherical micelles at these temperatures. This is a crude simple model that does not describe the PEO "whiskers" sticking out of the core region well but is good enough to obtain characteristic sizes. The core consists of hydrophobic PPO blocks while

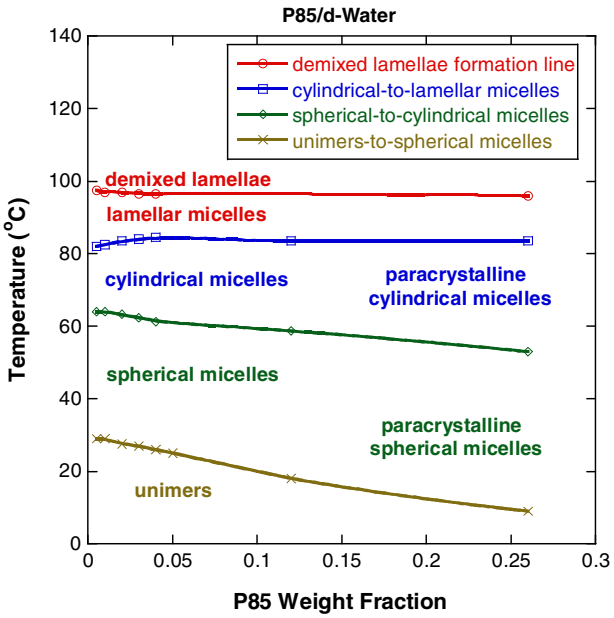

Fig. 10. Phase diagram for P85/d-water obtained from SANS measurements.

Author's personal copy

the shell contains the hydrophilic PEO blocks as well as hydration water. The SANS cross section for a spherical core of radius R_A (region A), a shell of radius R_B (region B) in a sea of solvent (region C) is given by:

$$\left[\frac{d\Sigma(Q)}{d\Omega}\right] = \frac{N}{V}[(\rho_A-\rho_C)V_A F(QR_A)+(\rho_B-\rho_C)(V_{A+B}F(QR_B) - V_A F(QR_A))]^2 S_I(Q) = \frac{N}{V}[(\rho_A-\rho_B)V_A F(QR_A) + (\rho_B-\rho_C)V_{A+B}F(QR_B)]^2 S_I(Q). \quad (4)$$

The following parameters have been defined. N is the number of core-shell particles in the solution, $\rho_A$is the scattering length density for region A, ρ_B is the scattering length density for region B, ρ_C is the scattering length density for region C, V_A is the volume of region A ($V_A = (4\pi/3)R_A{}^3$), V_{A+B} is the volume of regions A and B together ($V_{A+B} = (4\pi/3)R_B{}^3$), and V is the total sample volume.

The form factor amplitudes for spherical shapes are expressed in terms of the spherical Bessel function as:

$$F(QR_A) = \frac{3j_1(QR_A)}{QR_A}, \quad F(QR_B) = \frac{3j_1(QR_B)}{QR_B}. \quad (5)$$

$S_I(Q)$ is the inter-micelle structure factor modeled using the Percus–Yevick closure of the Ornstein–Zernike equation. The effect of particle size polydispersity is included through a Schulz distribution.

Using the polydisperse spherical core-shell model (NCNR SANS data analysis package), nonlinear least-squares fits were performed for each of the temperatures. Results for the 40 °C data are included here.

$$\begin{aligned}&\text{Packing volume fraction } \phi = 0.248\\ &\text{Core radius } R_A = 43.96 \text{ Å}.\\ &\text{Polydispersity parameter } \sigma_A/R_A = 0.16\\ &\text{Shell outer radius } R_B = 72.91 \text{ Å}\\ &\rho_A = 7.563\times10^{-7} \text{ Å}^{-2}\\ &\rho_B = 5.940\times10^{-6} \text{ Å}^{-2}\\ &\rho_C = 6.40\times10^{-6} \text{ Å}^{-2} \text{ (fixed for d-water)}.\end{aligned} \quad (6)$$

The micelles packing volume fraction is related to the number density as $\phi = NV_{A+B}/V$ where V_{A+B} is the micellar volume and V is the sample volume. These results are used in conjunction with material balance equations in the next section.

8. Material balance equations

The micelle core contains hydrophobic PO blocks and a fraction f of the EO blocks and the shell contains the remaining fraction (1-f) of the EO blocks. We assume that D_2O exists in the core (small amount) and in the shell to hydrate the EO blocks. We also assume that there are y_A D_2O molecules per EO monomer in the core (region A) and y_B D_2O molecules per EO monomer in the shell (region B). Define N_{agg} to be the aggregation number, i.e., the number of P85 molecules per micelle and recall that there are 40 PO monomers per block and 26 × 2 = 52 EO monomers per macromolecule. v_{EO}, v_{PO} and v_{D_2O} are the monomer volumes, respectively.

The material balance equations are:

$$\begin{aligned}&(1)\quad \frac{4\pi}{3}R_A^3 = N_{ag}\cdot[40\cdot v_{PO} + 52\cdot f\cdot v_{EO} + 52\cdot f\cdot v_{D_2O}\cdot y_A]\\ &(2)\quad \frac{4\pi}{3}(R_B^3 - R_A^3) = N_{ag}\cdot[52\cdot(1-f)\cdot v_{EO} + 52\cdot(1-f)\cdot v_{D_2O}\cdot y_B]\\ &(3)\quad \rho_A = \frac{N_{ag}[40b_{PO} + 52\cdot b_{EO}\cdot f + 52 b_{D_2O}\cdot f\cdot y_A]}{\frac{4\pi}{3}R_A^3}\\ &(4)\quad \rho_B = \frac{N_{ag}[52\cdot b_{EO}\cdot(1-f) + 52\cdot b_{D_2O}\cdot(1-f)\cdot y_B]}{\frac{4\pi}{3}\left(R_B^3 - R_A^3\right)}.\end{aligned} \quad (7)$$

These four linear equations can be solved to obtain:

$$\begin{aligned}y_B &= \frac{b_{EO} - v_{EO}\rho_B}{-b_{D_2O} + v_{D_2O}\rho_B}\\ y_A &= \frac{A + Bf}{f}\end{aligned} \quad (8)$$

where

$$\begin{aligned}A &= \frac{[52v_{EO} + 52y_B v_{D_2O}]\frac{R_A^3}{R_B^3 - R_A^3} - 40v_{PO}}{52v_{D_2O}}\\ B &= \frac{[-v_{EO} - y_B v_{D_2O}]\frac{R_A^3}{R_B^3 - R_A^3} - v_{EO}}{v_{D_2O}}\end{aligned} \quad (9)$$

$$f = \frac{E-C}{D-F}$$

and

Table 1
Scattering lengths densities for PO, EO and D_2O.

	Density (g/cm^3)		m_w (g/mol)	Molar volume (cm^3/mol)	Scattering lengths (cm)	Scattering length densities (Å^{-2})
PO	1.004	C_3H_6O	58	v_{PO} = 57.77	$b_{PO} = 3.307\times10^{-13}$	$\rho_{PO} = 3.44\times10^{-7}$
EO	1.127	C_2H_4O	44	v_{EO} = 39.04	$b_{EO} = 4.139\times10^{-13}$	$\rho_{EO} = 6.38\times10^{-7}$
D_2O	1.11	D_2O	20	v_{D_2O} = 18.02	$b_{D_2O} = 19.145\times10^{-13}$	$\rho_{D_2O} = 6.39\times10^{-6}$

The results for the 10% P85 in D_2O at 40 °C are included here.
f = 0.53 (53% of the EO monomers are in the core).
y_A = 0.39 (there is less than one D_2O molecule per EO monomer in the core).
y_B = 26.44 (there are 26.44 D_2O molecules per EO monomer in the shell).
N_{agg} = 59.80 (there are 59.80 P85 molecules per micelle).

Author's personal copy

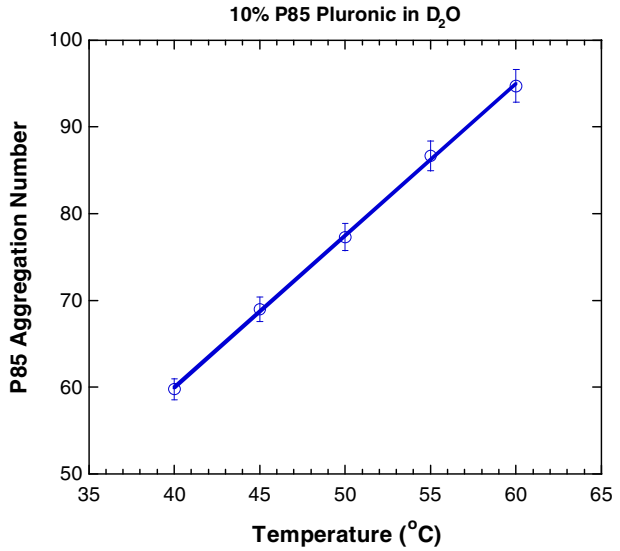

Fig. 11. Variation of the aggregation number with temperature. A line fit has been added as a trends guide. The error bars correspond to one standard deviation.

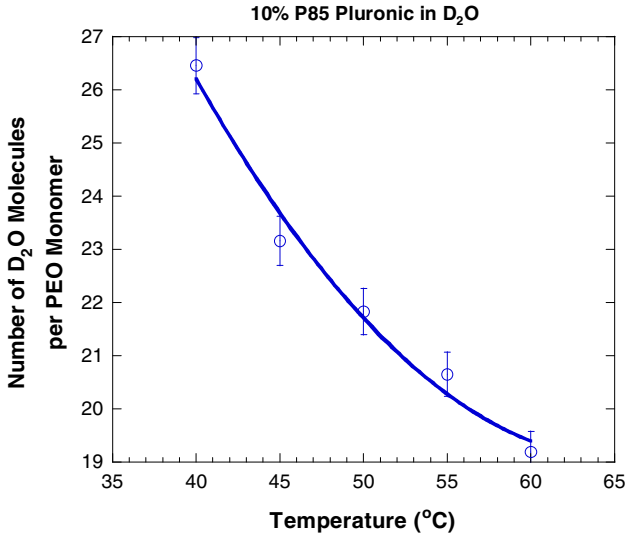

Fig. 12. Variation of the number of D_2O molecules per EO monomer in the shell region with increasing temperature. A second degree polynomial fit has been included as a guide to the eye.

$$\begin{aligned} C &= [40v_{PO} + 52 \cdot A \cdot v_{D_2O}]\rho_A \\ D &= [52v_{EO} + 52 \cdot B \cdot v_{D_2O}]\rho_A \\ E &= [40b_{PO} + 52 \cdot A \cdot b_{D_2O}] \\ F &= [52b_{EO} + 51 \cdot B \cdot b_{D_2O}]. \end{aligned} \tag{10}$$

The last parameter (the aggregation number) is given by:

$$N_{ag} = \frac{\frac{4\pi}{3}R_A^3}{40v_{PO} + 52v_{EO} \cdot f + 52v_{D_2O} \cdot f \cdot y_A}. \tag{11}$$

Table 1 summarizes known sample characteristics used to calculate neutron scattering length densities.

The aggregation number is seen to increase with increasing temperature in Fig. 11.

The number of d-water molecules per EO monomer in the shell region y_B is plotted in Fig. 12. It is seen to decrease with temperature as expected.

9. Summary

The phase behavior of Pluronic P85 was investigated in d-water. Below the critical micelle formation condition, unimers (dissolved polymers) are observed. Above that condition, micellar phases form. These are accompanied by an increase in the SANS intensity as well as structural transitions. For instance, transitions from spherical micelles to cylindrical micelles to lamellar micelles are easily identified. A demixed lamellae phase has also been observed. An empirical Guinier–Porod model used to analyze SANS data catches most of the qualitative features observed. A phase diagram for P85/d-water has been obtained using the various clues and the nonlinear least-squares fits.

The formation of spherical micelles is driven by the increasing hydrophobicity of PO monomers. Once the spherical micelles are formed, the EO monomers start becoming hydrophobic due to the break up of hydrogen bonds with water. This drives transitions to cylindrical micelles then to lamellar micelles with increasing temperature. Water is getting squeezed out of the EO-rich shell region more and more. At the highest temperature, most of the water gets squeezed out prompting the formation of the demixed lamellae phase. The observed micellar transitions are driven by the copolymer nature of P85 (hydrophobic PPO and hydrophilic PEO) while the demixed lamellae phase is driven by the demixing (phase separation) of PEO itself at the highest temperature.

Acknowledgments

The identification of commercial products does not imply endorsement by the National Institute of Standards and Technology nor does it imply that these are the best for the purpose. This work is based upon activities supported in part by the National Science Foundation under Agreement No. DMR-0944772. Discussions with Steve Kline are appreciated.

References

[1] Hammouda B. A new Guinier–Porod model. J Appl Crystallogr 2010;43:716–9.
[2] Glatter O, Kratky O. Small-angle X-ray scattering. Academic Press; 1982.
[3] Hansen JP, Verlet L. Phase transitions of the Lennard–Jones system. Phys Rev 1969;184:151.
[4] Mortensen K. Structural studies of aqueous solutions of PEO–PPO–PEO triblock copolymers: their micellar aggregates and mesophases; a SANS study. J Phys Condens Matter 1996;8:A13.
[5] Hammouda B. Probing nanoscale structures – the SANS toolbox; 2009. Available from: http://www.ncnr.nist.gov/staff/hammouda/the_SANS_toolbox.pdf.